AMATH 456

Mathematical Modelling of Shape Memory Alloys and their Applications in Aerospace

Group 3

Finn Dodgson
Michael Imseis
Rena Kaya
Emrys Halbertsma

December 17, 2020

Contents

Introduction

Abstract

Shape memory alloys (SMAs) have been adapted as sensors or actuators in a number of aerospace technologies. SMAs can exhibit unique hysteretic behaviours due to the non-convex nature of their free energy functions. We begin with a discussion of SMAs and their properties, followed by a decription of variational approaches to modeling SMAs in Chapter 2. Next, we offer some examples of the numerous applications of SMAs as sensors and actuators in the aerospace industry, including present and future uses. Finally, we briefly outline the formalism behind a continuous time model relevant to numerical simulation and discuss a computational model of Nitinol.

Key Words: Shape-Memory Alloys, Smart Materials, memory property, strain, stress, polycristalline, hysteresis.

1.1 Historical Background

In their article Memory Metal [1], George B. Kauffman and Issac Mayo tell about how scientist and engineer William J. Buehler discovered the peculiar "memory" property exhibited by a nickel-titanium alloy, under conditions which likely describe a large portion of scientific discoveries: "A lot of work and a little luck". After returning from World War II, Buehler started experimenting in his lab with different compounds chosen from the book *The Constitution of Binary Alloys* to find a fatigue-, impact-, and heat-resistant alloy to be used in the cone of a missile.[1] After working a considerable amount of time in his laboratory (according to the article Metal with Memory [2], he worked from 4:00AM to 11:00PM in an effort to seek solace in his lab during his separation from his wife), Buehler realized that one of the alloys (nickel-titanium, now commonly known as Nitinol) seemed to be considerably more durable than the rest that he tested. Later on, in a demonstration of durability shown on strips of metal alloys, he folded the strips into an accordion shape and passed it around among the attendees for them to observe this durability themselves. After one attendee, Dr. David S. Muzzey tried heating the strip with his pipe lighter, to everyone's surprise, the strip stretched out back to its original shape [1]. This curious discovery of the so-called "memory property" (observed in other materials as well) was then studied by many scientists and engineers. Today, shape-memory alloys, which fall under the class of smart materials, are used in numerous areas such as aerospace, robotics and (quite ironically, given Buehler's initial goal) medicine.

1.2 Properties of Shape Memory Alloys

The unique nature of SMAs arises from their ability to recover from up to 10% strains due to temperature or stress-induced deformations. This is because SMAs can exist in two distinct, thermodynamically stable phases: austenite and martensite [3]. Transitions between these two phases account for two key properties of SMAs, namely the *shape memory* and *pseudo-elastic* effects.

Firstly, consider the cooling and reheating of a SMA sample in the absence of any applied load. At a high temperature, the sample is in the cubic austenite phase. Upon cooling, the lattice reconfigures to the twinned martensite phase, as depicted in figure 1.1 below. When reheated, the sample returns to the austenite phase. Hence, the SMA is able to "remember" its original configuration in the austenite phase. We denote the temperatures at which the phase transitions begin and end as M_s, M_f, A_s, and A_f for the martensite (M) and austenite (A) phases, respectively [3]. The subscripts s and f are used to distinguish between the temperatures at which the phase transformations "start" and "finish". It should be noted here that depending on the alloy used, these temperatures can be tuned to values suited to a particular application.

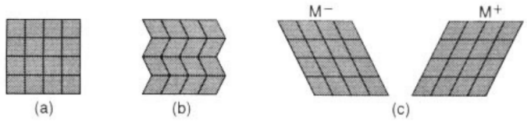

Figure 1.1: Schematic representation of the three phases of a shape memory alloy: (a) austenite, (b) twinned martensite, and (c) detwinned martensite variants.

If an external stress is applied to the sample, the resulting phase transformation is dependent upon the temperature of the environment. If the temperature is greater than A_f, then the sample is initially in the austenite phase and exhibits an approximately linear (elastic) stress-strain relationship. Once the stress attains a critical value σ_M, it becomes energetically favourable for the sample to transition to the detwinned martensite phase [3]. When the stress is decreased, the stress-strain curve again becomes approximately linear until the lower critical value of σ_A is reached. At this point, the material begins to revert to the austenite configuration and the sample fully recovers its initial shape. Conversely if the temperature is below M_f, the material begins in the twinned martensite state and will not return to its austenite form. Instead, it retains some 'plastic' or residual strain upon unloading. The sample must be heated above A_f to undergo complete shape recovery. A graphical representation of these two cases is shown in figure 1.2 below.

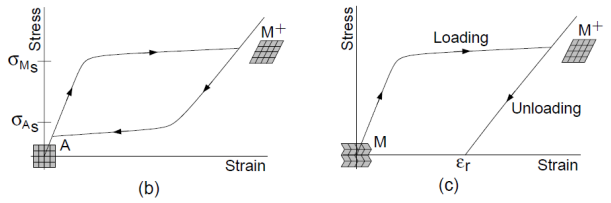

Figure 1.2: Adapted from figure 1.18 in [3]. In (b) we see the stress-strain curve subject to external loading/unloading when $T > A_f$. (c) depicts the curve when $T < M_f$. Notice that in (c), the sample begins in the twinned martensite (M) state and retains some residual strain ε_r upon unloading.

The ability of an SMA to return to its original shape upon removal of external stress in the high-temperature regime (Figure 1.2 (b)), is known as the *pseudoelastic* or *superelastic* effect.

Materials that have been classified as SMAs (in addition to NiTi) include alloys of: Copper-aluminium- nickel (CuAlNi), copper-zinc-aluminium (CuZnAl), and iron- manganese-silicon (FeMnSi) [3]. Nitinol is perhaps the most well-known and widely used of these.

1.3 Exhibition of Hysteretic Behavior in Shape Memory Alloys

Many of the properties that make shape memory alloys (SMAs) a topic of interest are classified under the phenomenon called hysteresis. Along with SMAs, some of the various systems that exhibit hysteretic behavior are cell signaling, an electronic comparator or a beam in a magnetic field [4]. In the article named What is Hysteresis?, Morris points out the lack of a general definition for this phenomenon and suggests a definition based on the system dynamics and operation in contrast to the existing definitions that are specific to different classes of systems [4].

The term *hysteresis* (which roughly translates from Greek as "to lag behind") was first used in the paper Experimental Researches in Magnetism [4]. The core properties of SMAs (and other smart materials) are results of hysteretic behaviors, namely its memory property and the *rate independence* of operation. These materials transform one form of energy into another. Temperature driven SMAs turn thermal energy into mechanical energy while magnetostrictives (including magnetic SMAs) transform magnetic work into mechanical energy, yet the two systems have the same inherent memory and rate independence properties. Qualitatively, rate independence means that the output of the system is only dependent on the system input and not on how quickly the input is being varied [4]. The complete dependence of the input-output graph on the input makes it appear as if the system "remembers" its initial state, giving rise to the *memory property*.

1.3.1 Analyzing the Hysteretic Behavior of a Magnetostrictive Material

In an effort to construct a more abstract definition of hysteresis, Morris examines various systems that are said to exhibit hysteresis; one of them being the response of a magnetostrictive material to an external magnetic field [4]. In the model, the magnetostrictive material (some examples of which include the alloys Terfenol-D and Galfenol) is thought to be composed of magnetic dipoles. Qualitatively, the Gibbs energy function for dipoles of different values of external magnetic fields are given. When there is no field applied, the system has a symmetric energy function. As the strength of the external magnetic field is increased, the energy function tends towards a polarized, asymmetric configuration favoring one stable point over the other until only one equilibrium point remains (see Figure 1.3). Following Hamilton's principle, "Between fixed times a and b, a system moves along the trajectory that makes stationary the action integral over all admissible trajectories"[5]. The symmetry of the system is tunable and the system is naturally driven to the equilibrium points, making it possible (in a sense) to "initialize" the material with each dipole setting being one of the two equilibrium points. This uniqueness that gives rise to the memory property of magnetostrictive materials is ultimately a result of the energy function of the dipoles being non-convex. By Proposition 2.15 of the course notes, if J is convex, then any stationary point of J in D minimizes J on D.[5] Hence, if J were convex everywhere, there could not be a local maximum in between the two stable equilibria (or in fact, anywhere) to give rise to an adjustable binary system. The state possessing high symmetry corresponds to austenite and the state with lower symmetry

corresponds to martensite [3].

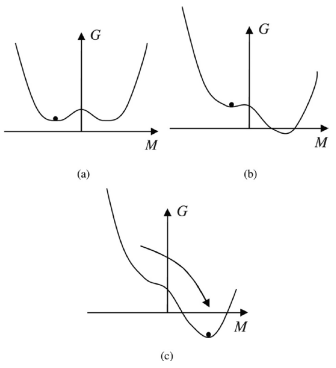

Figure 1.3: The value of H_0 is 0 in (a) and is gradually increased. The system starts favoring one equilibrium point over the other in (b), until there is only one equilibrium left in (c). [4]

Before building a macro model, it is insightful to first describe the mathematics on the micro scale as in the Homogenized Energy approach (see Chapter 2 for more detail). A dipole in a magnetostrictive material is governed by the minimization of the Gibbs free energy, which is defined through the function $f(M)$ and ultimately through the Helmholtz energy, defined in [4] as:

$$\Psi(m,\varepsilon) = \frac{1}{2}y\varepsilon^2 - Y\gamma_1\varepsilon M^2 + f(M), \tag{1.1}$$

where

$$f(M) = \begin{cases} \frac{\mu_0\eta}{2}(M+M_R)^2, & M \le -M_I, \\ \frac{\mu_0\eta}{2}(M_R - M_I)(M_R - \frac{M^2}{M_I}) & |M| < M_I, \\ \frac{\mu_0\eta}{2}(M-M_R)^2, & M \ge M_I. \end{cases} \tag{1.2}$$

In equations (1.1) and (1.2) , M is the magnetization of the dipole, ε is the total strain, and M_R η, γ_1 and Y are physical constants. M_R is determined experimentally and plays a crucial mathematical role, as $\pm M_R$ give the deviation of the equilibrium points from $\frac{H_0}{\eta}$, which create the two "states" for the case with no applied magnetization. The presence of this physical constant is a key property that makes smart materials fine tunable.

$$G(H_0, M, \sigma, \varepsilon) = \Psi(m,\varepsilon) - \mu_0 H_0 M \tag{1.3}$$

To find the equilibrium points, the Gibbs free energy given in (1.3) is partially differentiated with respect to the magnetization M (for the case where $|M| < M_I$) to yield the locations of equilibria and the critical value H_c after which the system posseses only one equilibrium. This calculation gives:

$$M_+^* = \frac{H_0}{\eta} + M_R, \tag{1.4}$$

$$M_-^* = \frac{H_0}{\eta} - M_R, \tag{1.5}$$

$$H_c = \eta(M_R - M_I), \tag{1.6}$$

according to [4]. With these expressions, it is now clear how to shift the system from two equally favored equilibria to only one on the micro scale by vayring the external field. If the system can respond to changes in the field fast enough (the idealization of which is called rate-independence), it has the potential to exhibit the exotic hysteretical behaviors. Having set up an abstract mathematical background, following the analysis of this example and various others, the paper suggests a general definition as follows: "A hysteretic system is one which has (1) multiple stable equilibrium points and (2) dynamics that are considerably faster than the time scale at which inputs are varied." [4] After establishing the model on the micro scale, material behaviour on the macro scale can be investigated by way of homogenization techniques or by other means.

Theoretical Background

There are several different ways in which a variational approach to modelling SMAs can be taken. Generally, the models discussed here fall under the umbrella of 'Homogenized Energy Models' as described in [3]. The basic idea is to balance the "the Gibbs and thermal energies through Boltzmann [thermodynamic] principles in single crystal compounds." The homogenization refers to the fact that the theory begins with relations describing the material at the lattice-level (or mesoscale), and is then integrated over a distribution to yield a macroscopic model. Particularly, as Smith explains, "lattice variations, polycrystallinity, and variable stresses are subsequently incorporated by assuming that parameters such as relative and effective stresses are manifestations of underlying distributions rather than constants" [3][1]. Meaning these values are functions of model parameters such as T or ε (see section 2.1.2). Thus, the model at once incorporates both micro- and macroscopic features to effectively simulate the material behaviour.

2.1 Thermodynamic Energy Relations

Here we present a homogenization approach for uniaxial SMA behaviour. As mentioned, a driving principle is the balancing of Gibbs and Helmholtz energies. The Gibbs free energy is given by

$$G(\sigma, \varepsilon, T) = \psi(\varepsilon, T) - \sigma\varepsilon, \tag{2.1}$$

where $\psi(\varepsilon, T)$ is the Helmholtz energy, T is the temperature, and ε is the uniaxial shear strain. The equilibrium value for ε is $\varepsilon = 0$ for austenite and $\varepsilon = \varepsilon_T$ for detwinned martensite in the absence of external stress. As seen in figure 1.1 (c), the detwinned martensite possesses some shear strain by default, whether positive or negative [3].

There exist a number of choices for $\psi(\varepsilon, T)$ depending on the features and level of detail that the model seeks to capture. The trade-off for higher accuracy is of course an increased number of undetermined parameters and hence a greater computational challenge. The lowest-order polynomial expansion that exhibits first-order phase transitions,[2] is the sixth-degree Falk polynomial,

$$\psi(\varepsilon, T) = \psi_0(T) + \alpha_1(T - T_0)\varepsilon^2 - \alpha_2\varepsilon^4 + \alpha_3\varepsilon^6, \tag{2.2}$$

where $\alpha_1, \alpha_2, \alpha_3$ are positive constants and T_0 is the Curie temperature (the point above which the SMA loses its permanent magnetic properties). Typically, the first term is taken to be $\psi_0(T) = -TS$ where S is the specific entropy. ψ can also be defined as a higher order polynomial expansion or a piecewise C^1 function.

Equivalent to the second law of thermodynamics, the principle of minimum energy states that a closed system with a fixed entropy will minimize the total energy at equilibrium [7]. Consequently, at a given temperature and external stress, the material strains will react such that $G(\sigma, \varepsilon, T)$ is minimized. Necessary conditions for the minimization of G are

$$\frac{\partial G}{\partial \varepsilon} = 0, \quad \frac{\partial^2 G}{\partial \varepsilon^2} > 0, \tag{2.3}$$

the first of which implies

$$\frac{\partial \psi}{\partial \varepsilon} = \sigma, \tag{2.4}$$

by equation (2.1). Accordingly, one can obtain a constitutive relation between the stress σ and the shear strain ε by differentiating (2.2) and setting it equal to σ. This relation can then be used to draw a predicted stress-strain curve. For examples at different temperatures, see figure 2.1 below.

It is worth noting that the second condition in (2.3) implies that G is strictly convex, meaning the material will achieve a unique minimizing state at equilibrium.

[1] *Polycrystallinity* refers to the presence of crystal structures in varying orientations in the bulk of the material.

[2] In the Ehrenfest classification system, phase transitions are labeled by the lowest order derivative for which the free energy is discontinuous [6]. (i.e. the first derivative of ψ is discontinuous for 1^{st}-order phase transition such as solid to liquid.)

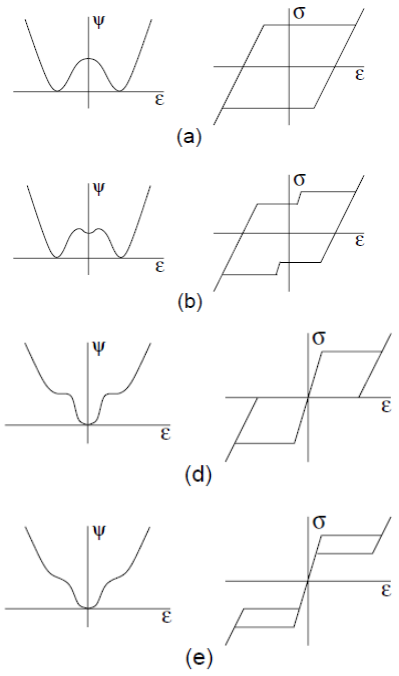

Figure 2.1: ψ and σ-ε curves given by 2.3-2.4. (a) $T < T_0$: shape memory effect is observed, in (d) $T = T_1$[3]: pseudoelastic behaviour begins to be observed, (b) and (e) both show intermediate states at lower and higher temperatures respectively [3].

Figure 2.2 shows the Gibbs free energy for a fixed temperature in the austenite regime ($T > A_f$) at $\sigma = 0$ as well as the critical stress values σ_M, where the transition to martensite begins, and σ_A where the reverse process occurs upon unloading. Figure 2.2 (b) is a plot of the local stress-strain curve for the same temperature (similar to figure 2.1 (e)), neglecting thermal activation (kT/V is small). Finally, figure 2.2 (c) shows the stress-strain curve incorporating the effects of thermal activation on the phase transitions, which results in a 'smoothing' of the graph at the transition points; closer to what is observed experimentally.

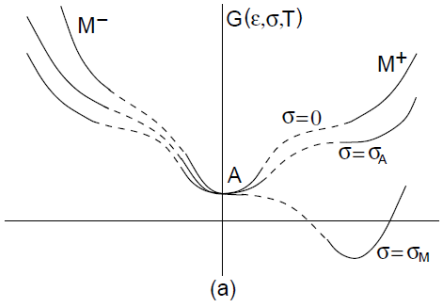

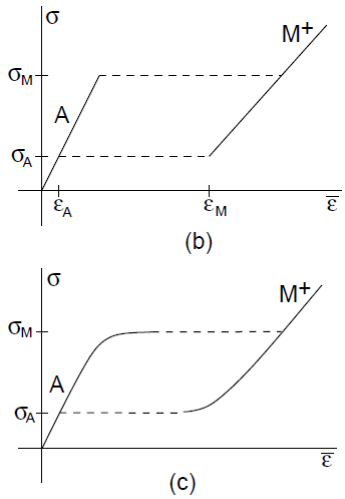

Figure 2.2: Gibbs energy and stress-strain curves resulting from 2.1 (a), 2.3 (b), and consideration for thermally-activated phase transitions (c). Retrieved from [3].

In order to "incorporate nonlocal effects such as interfacial energies or domain wall effects," one can augment the Helmholtz energy by the addition of the gradient term ε_x^2 [3]. The interfacial or surface energy refers to the excess energy present in lattice elements at a surface compared to those in the bulk, due to the surface being less energetically favourable.

$$\tilde{\psi}(\varepsilon, \varepsilon_x, T) = \psi(\varepsilon, T) + \frac{\gamma}{2}\varepsilon_x^2. \tag{2.5}$$

2.1.1 Shear Strains of an SMA Rod

As an illustrative example, we can now consider the case of an SMA rod of length ℓ and cross-sectional area A, subject to an applied force $f(t, x)$. If u is the longitudinal displacement of the rod, then ε is related to u by

$$\varepsilon(t, x) = \frac{\partial u}{\partial x}(t, x), \tag{2.6}$$

and the total free energy of the system is

$$U(t) = A \int_0^\ell \left[\psi(\varepsilon(t,x), T) + \frac{\gamma}{2}\varepsilon_x^2(t,x) - \rho u(t,x) f(t,x) \right] \mathrm{d}x. \tag{2.7}$$

The kinetic energy is

$$K(t) = A \int_0^\ell \frac{\rho}{2} u_t^2(t,x) \mathrm{d}x. \tag{2.8}$$

The Lagrangian is $\mathcal{L} = K - U$ and the action is

$$\mathcal{A} = \int_a^b \int_0^\ell \left(\frac{\rho}{2}u_t^2 - \psi(\varepsilon, T) - \frac{\gamma}{2}\varepsilon_x^2 + \rho u f \right) \mathrm{d}x\mathrm{d}t. \tag{2.9}$$

[3] At $T_1 = A_f$ the SMA defaults to the austenite phase, though martensite variants can be induced by sufficiently large stresses.

By Hamilton's principle, the displacement u will make stationary the action. We begin by finding the Gateaux derivative of the action, considering a variation $v(t,x)$. Making the substitution $\varepsilon = u_x$ (by 2.6),

$$\mathcal{A} = \int_a^b \int_0^\ell \left(\frac{\rho}{2} u_t^2 - \psi(u_x, T) - \frac{\gamma}{2} u_{xx}^2 + \rho u f \right) \mathrm{d}x\mathrm{d}t. \tag{2.10}$$

Since ψ is a continuous function, $\mathcal{A}(u+\epsilon v)$ is continuous in ϵ (and is defined for $\epsilon = 0$). Hence, we can compute the variation of $\mathcal{A}$ by taking the derivative,

$$\begin{aligned}
\delta\mathcal{A}(u;v) &= \frac{\partial \mathcal{A}}{\partial \epsilon}(u+\epsilon v)\bigg|_{\epsilon=0} \\
&= \frac{\partial}{\partial \epsilon} \int_a^b \int_0^\ell \bigg(\frac{\rho}{2}(u_t + \epsilon v_t)^2 - \psi(u_x + \epsilon v_x, T) \\
&\quad - \frac{\gamma}{2}(u_{xx} + \epsilon v_{xx})^2 + \rho(u+\epsilon v) f \bigg) \mathrm{d}x\mathrm{d}t \bigg|_{\epsilon=0} \\
&= \int_a^b \int_0^\ell \bigg(\rho u_t v_t - \frac{\partial \psi}{\partial \varepsilon}(u_x, T) v_x - \gamma u_{xx} v_{xx} \\
&\quad + \rho v f \bigg) \mathrm{d}x\mathrm{d}t
\end{aligned}$$

Next, apply integration by parts. We assume that all boundary terms vanish, as they depend on any given boundary values and will simply yield different natural boundary conditions depending on the situation.

$$\begin{aligned}
\delta\mathcal{A}(u;v) &= \int_0^\ell \int_a^b \rho u_t v_t \mathrm{d}t\mathrm{d}x - \int_a^b \int_0^\ell \frac{\partial \psi}{\partial \varepsilon} v_x \mathrm{d}x\mathrm{d}t \\
&\quad \int_a^b \int_0^\ell \gamma u_{xx} v_{xx} \mathrm{d}x\mathrm{d}t + \int_a^b \int_0^\ell \rho v f \mathrm{d}x\mathrm{d}t \\
&= \int_0^\ell \left(\rho u_t v \bigg|_a^b - \int_a^b \rho u_{tt} v \mathrm{d}t \right) \mathrm{d}x \\
&\quad - \int_a^b \left(\frac{\partial \psi}{\partial \varepsilon} v \bigg|_0^\ell - \int_0^\ell \frac{\partial}{\partial x}\left(\frac{\partial \psi}{\partial \varepsilon} \right) v \mathrm{d}x \right) \mathrm{d}t \\
&\quad - \int_a^b \left(\gamma u_{xx} v_x \bigg|_0^\ell - \int_0^\ell \gamma u_{xxx} v_x \mathrm{d}x \right) \mathrm{d}t \\
&\quad + \int_a^b \int_0^\ell \rho v f \mathrm{d}x\mathrm{d}t
\end{aligned}$$

Collecting terms and applying integration by parts with respect to x once again on the third term,

$$\begin{aligned}
\delta\mathcal{A}(u;v) &= \int_a^b \int_0^\ell \left(-\rho u_{tt} + \frac{\partial}{\partial x}\left(\frac{\partial \psi}{\partial \varepsilon} \right) + \rho f \right) v \mathrm{d}x\mathrm{d}t \\
&\quad + \int_a^b \left(\gamma u_{xxx} v \bigg|_0^\ell - \int_0^\ell \gamma u_{xxxx} v \mathrm{d}x \right) \mathrm{d}t \\
&= \int_a^b \int_0^\ell \bigg(- \rho u_{tt} + \frac{\partial}{\partial x}\left(\frac{\partial \psi}{\partial \varepsilon} \right) + \rho f \\
&\quad - \gamma u_{xxxx} \bigg) v(t,x) \mathrm{d}x\mathrm{d}t
\end{aligned}$$

Since the variation v is arbitrary, this means that $u(t,x)$ must satisfy the partial differential equation:

$$\rho u_{tt} - \frac{\partial}{\partial x}\left(\frac{\partial \psi}{\partial \varepsilon} \right) + \gamma u_{xxxx} = \rho f(t,x) \tag{2.11}$$

where ψ is given by (2.2) or an equivalent Helmholtz energy. Equations which govern the transfer of heat within an SMA sample over time may also be derived. However, these are considerably more complicated than the example given here and are hence not included.

2.1.2 Homogenized Energy Model

A common approach taken when considering simple SMA configurations with a high degree of symmetry, such as wires, rods, or thin films, is to treat the sample as being comprised of varying fractions of austenite and martensite phases [3]. For simplicity, we consider austenite (A) and detwinned martensite (M^+, M^-) lattice elements. Denote the total volume fractions of A, M^+, and M^- as $x_A(t)$, $x_+(t)$, and $x_-(t)$ respectively such that $x_A + x_+ + x_- = 1$ at all times. Taking the thermal activation of phase transitions into account, it is possible to develop rate equations for x_A, x_+, and x_-. (See section 5.5.1 in [3] for details.) Then, in the case of significant thermal activation, the local average strains are characterized by

$$\bar{\varepsilon} = \langle \varepsilon_- \rangle x_- + \langle \varepsilon_+ \rangle x_+ + \langle \varepsilon_A \rangle x_A \tag{2.12}$$

As mentioned, to account for material inhomogeneities and lattice variations in going from the mesoscopic to macroscopic model, we treat the relative and effective stresses as distributions. The relative stress is defined as the difference

$$\sigma_R(T) = \sigma_M(T) - \sigma_A(T) \tag{2.13}$$

where the transformation stresses σ_M and σ_A are those described in section 1.2. Additionally, the effective stress in the material, σ_e is the combination of the applied stress and stresses due to local interactions in the lattice, σ_I.

$$\sigma_e = \sigma + \sigma_I \tag{2.14}$$

To characterize the non-constant nature of σ_R and σ_e, we define two underlying densities ν_1 and ν_2. Possible choices for ν_1, ν_2 include:

$$\nu_1(\sigma_R) = c_1 e^{-[\ln(\sigma_R/\bar{\sigma}_R)/2c]^2} \tag{2.15}$$

which accounts for the fact that $\sigma_M \geq \sigma_A$, and so $\sigma_R \geq 0$. For ν_2 we have

$$\nu_2(\sigma_I) = c_2 e^{-\sigma_I^2/2b^2}, \text{ and} \tag{2.16}$$

$$\nu_2(\sigma_I) = c_2 e^{-|\sigma_I|/b}. \tag{2.17}$$

Equation (2.15) is known as a lognormal distribution, (2.16) is a 'normal density', and (2.17) is called a Laplace relation. Alternatively, ν_1 and ν_2 can be taken as general densities that satisfy the following conditions:

(i) $\nu_1(x)$ is defined for $x > 0$ (*positivity*)

(ii) $\nu_2(-x) = \nu_2(x)$ (*symmetry*)

(iii) $\left|\nu_1(x)\right| \leq c_1 e^{-a_1 x}$, $\left|\nu_2(x)\right| \leq c_2 e^{-a_2 x}$ (*integrability*)

Where $c_1, a_1, c_2, a_2 > 0$. Then, the time evolution of the bulk strains as a function of the input stress and temperature (these can be thought of as control variables) is governed by:

$$\varepsilon(\sigma, T; t) = \int_0^\infty \int_{-\infty}^\infty \nu_1(\sigma_R)\nu_2(\sigma_I)\bar{\varepsilon}(\sigma + \sigma_I, T; \sigma_R, t)\mathrm{d}\sigma_I \mathrm{d}\sigma_R$$

meaning we have arrived at a macroscopic relation descibing the stress-strain behaviour of the material subject to external stress σ and temperature T (which can depend on time). The function $\bar{\varepsilon}$ is as defined in equation (2.12).

2.2 Entropy Gradient Flow

Auricchio et al. [8], cast the problem as a generalized gradient flow of the total entropy, $S(\mathbf{y})$. This means that the system state satisfies,

$$\frac{\partial K(t, \mathbf{y}, \dot{\mathbf{y}})}{\partial \dot{\mathbf{y}}} - \nabla S = 0 \tag{2.18}$$

in the case of smooth K and S. K is defined as the *entropy production potential* and satisfies the condition: for all $(t, \mathbf{y})$, $\dot{\mathbf{y}} \mapsto K(t, \mathbf{y}, \dot{\mathbf{y}})$ is convex, non-negative, and $K(t, \mathbf{y}, \mathbf{0}) = 0$.

The approach taken here is based upon the General Equations for Non-Equilibrium Reversible-Irreversible Coupling (GENERIC) formalism for thermodynamic systems. The theory is specifically tailored to systems with both reversible and irreversible dynamics, including the hysteretic behaviour exhibited by SMAs [8]. Generally speaking, reversible processes relate to changes in free-energy, while irreversible processes relate to changes in entropy (as per the second law of thermodynamics).

2.2.1 Notation & Definitions

To model three-dimensional stresses and strains, it is necessary to make use of tensors. In keeping with [8], bold letters denote vectors and 2-tensors (which can be expressed as matrices) and double capital letters represent 4-tensors. 4-tensors can be thought of as higher-dimensional arrays with four indices. Given matrices $\boldsymbol{\alpha}, \boldsymbol{\beta} \in \mathbb{R}^{3\times3}$ and the tensor $\mathbb{A} \in \mathbb{R}^{3\times3\times3\times3}$, define the scalar product $\boldsymbol{\alpha} : \boldsymbol{\beta} \in \mathbb{R}$ as

$$\boldsymbol{\alpha} : \boldsymbol{\beta} \equiv \alpha_{ij}\beta_{ij}$$

and the product $\mathbb{A}\boldsymbol{\beta} \in \mathbb{R}^{3\times3}$ as[4]

$$(\mathbb{A}\boldsymbol{\beta})_{ij} \equiv A_{ijlk}\beta_{lk}$$

A majority of the tensors used here are symmetric, hence $\mathbb{R}^{3\times3}_{\text{sym}}$ is used to refer to the set of 3×3 symmetric 2-tensors. The trace is defined in the usual way, $\mathrm{tr}(\boldsymbol{\alpha}) = \alpha_{ii}$. Consistent with the earlier definition of the scalar product, the natural inner product for real, square matrices is

$$\boldsymbol{\alpha} : \boldsymbol{\beta} \equiv \mathrm{tr}(\boldsymbol{\alpha}\boldsymbol{\beta}^T) = \mathrm{tr}(\boldsymbol{\alpha}\boldsymbol{\beta})$$

since $\boldsymbol{\beta}$ is symmetric. This defines the scalar product on $\mathbb{R}^{3\times3}_{\text{sym}}$, with the corresponding norm $|\boldsymbol{\alpha}|^2 = \boldsymbol{\alpha} : \boldsymbol{\alpha}$. Finally, an important subspace of $\mathbb{R}^{3\times3}_{\text{sym}}$ is the set of *deviatoric* symmetric matrices, $\mathbb{R}^{3\times3}_{\text{dev}}$ given by $\{\alpha \in \mathbb{R}^{3\times3}_{\text{sym}} | \mathrm{tr}(\alpha) = 0\}$. Any symmetric matrix can then be decomposed into $\boldsymbol{\alpha} = \mathrm{dev}(\boldsymbol{\alpha}) + \frac{1}{3}\mathrm{tr}(\boldsymbol{\alpha})\mathbb{I}$ where $\mathrm{dev}(\boldsymbol{\alpha})$ is given by:

$$\mathrm{dev}(\boldsymbol{\alpha}) = \begin{pmatrix} \alpha_{11} - \tau & \alpha_{12} & \alpha_{13} \\ \alpha_{21} & \alpha_{22} - \tau & \alpha_{23} \\ \alpha_{31} & \alpha_{32} & \alpha_{33} - \tau \end{pmatrix}$$

with $\tau = \frac{1}{3}\mathrm{tr}(\boldsymbol{\alpha})$.

2.2.2 Free-Energy Density

Define $\mathbf{u} : \Omega \longrightarrow \mathbb{R}^3$ to be the displacement from the reference configuration of the sample, $\Omega \subset \mathbb{R}^3$. In the small-deformation regime, decompose the linearized strain,

$$\boldsymbol{\varepsilon}(\mathbf{u}) = \frac{1}{2}(\nabla\mathbf{u} + \nabla\mathbf{u}^T) \tag{2.19}$$

as

$$\boldsymbol{\varepsilon} = \boldsymbol{\varepsilon}^{el} + \mathbf{e}^{tr} \tag{2.20}$$

[4] These definitions make use of the Einstein summation convention: any repeated index in the expression is summed over, i.e. $\alpha_{ij}\beta_{ij} := \sum_{i=1}^3 \sum_{j=1}^3 \alpha_{ij}\beta_{ij}$

where $\boldsymbol{\varepsilon}^{el}$ is the elastic component of the strain and $\mathbf{e}^{tr}$ is the inelastic strain associated with transformation and reorientation of the martensitic domains. Particularly, $\mathbf{e}^{tr}$ acts as an internal variable to characterize the phase composition analogous to $x_{\pm}$ described in section 2.1.2 [3]. The value $|\mathbf{e}^{tr}|$ is then a measure of the martensitic content of the sample, which satisfies $|\mathbf{e}^{tr}| \leq \epsilon_L$ (where ϵ_L is the maximum strain that can occur due to martensitic reorientation) [8]. As the process is assumed to be isochoric, $\mathbf{e}^{tr}$ can therefore be assumed to be deviatoric.

The equilibrium of the Shape Memory Alloy is described by the free-energy density which can be defined as follows:

$$\psi(\boldsymbol{\varepsilon}, \mathbf{e}^{tr}, T) = cT(1 - \log T) + \frac{1}{2}(\boldsymbol{\varepsilon} - \mathbf{e}^{tr}) : \mathbb{C}(\boldsymbol{\varepsilon} - \mathbf{e}^{tr}) + \frac{H}{2}|\mathbf{e}^{tr}|^2 + f(T)|\mathbf{e}^{tr}| + \mathscr{I}(\mathbf{e}^{tr}) \quad (2.21)$$

where T is the temperature, which is assumed to be uniform for simplicity. Since $f(T)$ is the only term that depends on the temperature, this term encapsulates the thermomechanical coupling of the system. $\mathbb{C}$ is the isotropic elasticity tensor, which relates the stress and the elastic component of the strain via $\boldsymbol{\varepsilon}^{el} = \mathbb{C}^{-1}\boldsymbol{\sigma}$. The constant $c > 0$ is the specific heat capacity of the sample. H is a hardening parameter, associated with the elastic response of austenite and martensite (assumed to be the same for both variants). Finally, the indicator function $\mathscr{I} : \mathbb{R}^{3\times3}_{\text{dev}} \to [0, \infty]$ defined as

$$\mathscr{I}(\mathbf{e}^{tr}) = \begin{cases} 0 & \text{if } |\mathbf{e}^{tr}| \leq \epsilon_L \\ \infty & \text{otherwise} \end{cases} \quad (2.22)$$

serves to enforce the constraint that $|\mathbf{e}^{tr}| \leq \epsilon_L$ for finite energies. Seeing as $\mathbf{e}^{tr}$ is deviatoric, it can be convenient to re-express the free-energy in terms of the volumetric and deviatoric strains. That is, instead of (2.20), decompose the strain as

$$\boldsymbol{\varepsilon} = \left(\frac{v}{3}\right)\mathbb{I} + \mathbf{e} \quad (2.23)$$

Here, $v = \text{tr}(\boldsymbol{\varepsilon})$ represents the volumetric strain, $\mathbf{e} = \text{dev}(\boldsymbol{\varepsilon})$ is the deviatoric strain, and $\mathbb{I}$ is the identity 2-tensor.

Then, (2.21) becomes

$$\psi(v, \mathbf{e}, \mathbf{e}^{tr}, T) = cT(1 - \log T) + \frac{K}{2}v^2 + G|\mathbf{e} - \mathbf{e}^{tr}|^2 + \frac{H}{2}|\mathbf{e}^{tr}|^2 + f(T)|\mathbf{e}^{tr}| + \mathscr{I}(\mathbf{e}^{tr}) \quad (2.24)$$

[5] $q = \{v, \mathbf{e}, \mathbf{e}^{tr}, T\}$

$K, G > 0$ are the bulk modulus and shear modulus, respectively. Suppose $\Omega \subset \mathbb{R}^3$ is the volume occupied by the sample. Then, the total free energy is given by

$$\Psi(v, \mathbf{e}, \mathbf{e}^{tr}, T) = \int_\Omega \psi(v, \mathbf{e}, \mathbf{e}^{tr}, T)\text{d}V \quad (2.25)$$

The constitutive relations which govern the response of the material are then given by the variations of ψ with respect to its variables. Seeing as ψ is rate-independent, the second term of the Euler-Lagrange equation vanishes and the variation reduces to partial differentiation. For a given coordinate q,[5]

$$\delta\psi = \frac{\partial\psi}{\partial q} - \frac{d}{dt}\frac{\partial\psi}{\partial\dot{q}} \quad (2.26)$$

$$\delta\psi = \frac{\partial\psi}{\partial q} \quad (2.27)$$

Using equation (2.24), we obtain the four constitutive relations:

$$\frac{\partial\psi}{\partial v} = Kv \equiv p \quad (2.28)$$

$$\frac{\partial\psi}{\partial \mathbf{e}} = 2G(\mathbf{e} - \mathbf{e}^{tr}) \equiv \boldsymbol{S}_{\text{dev}} \quad (2.29)$$

$$\frac{\partial\psi}{\partial T} = -c\log T + f'(T)|\mathbf{e}^{tr}| \equiv -s \quad (2.30)$$

$$\frac{\partial\psi}{\partial \mathbf{e}^{tr}} = -\boldsymbol{S}_{\text{dev}} + H\mathbf{e}^{tr} + f(T)\partial|\mathbf{e}^{tr}| + \partial\mathscr{I}(\mathbf{e}^{tr}) \equiv -\boldsymbol{X} \quad (2.31)$$

Here, p is the pressure, $\boldsymbol{S}_{\text{dev}}$ is the deviatoric stress, s is the entropy density, and $\boldsymbol{X}$ is a thermodynamic variable associated with the internal variable $\mathbf{e}^{tr}$. The Cauchy Stress tensor can then be written as: $\boldsymbol{\sigma} = p\mathbb{I} + \boldsymbol{S}_{\text{dev}}$ [8]. The derivatives of $|\mathbf{e}^{tr}|$ and I are defined as follows:

$$\partial|\mathbf{e}^{tr}| = \begin{cases} \frac{\mathbf{e}^{tr}}{|\mathbf{e}^{tr}|} & \text{if } \mathbf{e}^{tr} \neq \mathbf{0} \\ \mathbf{0} & \text{if } \mathbf{e}^{tr} = \mathbf{0} \end{cases}$$

$$\partial\mathscr{I}(\mathbf{e}^{tr}) = \begin{cases} \mathbf{0} & \text{if } |\mathbf{e}^{tr}| < \epsilon_L \\ \xi\frac{\mathbf{e}^{tr}}{|\mathbf{e}^{tr}|}, \xi \geq 0 & \text{if } |\mathbf{e}^{tr}| = \epsilon_L \\ \varnothing & \text{if } |\mathbf{e}^{tr}| > \epsilon_L \end{cases} \quad (2.32)$$

We are now in a position to formulate the entropy as a functional. If we take $\mathbf{y} = (\mathbf{e}^{tr}, T)$ then by (2.30), the total entropy is:

$$S(\mathbf{y}) = \int_\Omega s(\mathbf{y})\text{d}x = \int_\Omega (c\log T - f'(T)|\mathbf{e}^{tr}|)\text{d}x \quad (2.33)$$

and the gradient is

$$\nabla S = \begin{pmatrix} -f'(T)\partial|\mathbf{e}^{tr}| \\ c/T - f''(T)|\mathbf{e}^{tr}| \end{pmatrix} \tag{2.34}$$

This can then be used to determine the system state via equation (2.18). For more details and suitable choices of K and f the reader is referred to [8].

2.3 Extension to Modelling Magnetic SMAs

2.3.1 Defining the Energy Functional

An interesting class of SMAs are the so called *Magnetic* SMAs (MSMAs). These are materials that can undergo heavy and reversible strains when subjected to an external magnetic field. Among the various MSMAs, the most widely studied is the NiMnGa alloy [9, 10, 11]. Methods from variational calculus can be used to study these materials and it is the purpose of this section to give an example of how this works.

As in the case of standard SMAs, the system of equations that describe MSMAs can be derived by taking variational derivatives of an energy functional. The MSMA sample is set up such that it is in a single state before an external magnetic field is applied to it. Once the magnetic field is applied, the MSMA undergoes a transformation between two martensitic variant states, hereby called "variant 1" and "variant 2" with volume fraction $(1-\xi)$ and ξ, respectively. It is also worth pointing out that associated with each of these two variant states, there are two kinds of magnetic domains with respective volume fractions $(1-\alpha)$ and α.

The effective magnetization at a single point inside the MSMA can be defined as

$$\overline{\mathbf{M}} = M_s \left[(1-\xi)\sin\theta + \xi(2\alpha - 1)\right] \mathbf{e}_2 \tag{2.35}$$

where $\mathbf{e}_2$ is a unit vector along the y-axis and θ is the angle with which the magentization vector of the material rotates after the application of an external magnetic field. The magnetization of the MSMA will induce the distribution of a magnetic scalar potential $\Psi(\mathbf{X})$ in $\mathbb{R}^3$ [12].

Following [12], we first will define each term of the energy functional, before putting it all together.

First, the *elastic potential energy* is defined as

$$\mathcal{F}_{el} = \int_{\Omega_r} \rho_r \phi(\mathbb{F}, \xi) dV \tag{2.36}$$

where $\Omega_r \subset \mathbb{R}^3$ is the region that the MSMA occupies, ϕ is the elastic energy per unit mass, ρ_r is the density of the material, and $\mathbb{F}$ is called the deformation gradient tensor. ($\mathbb{F}$ is related to the displacement $\mathbf{u}$ by $\mathbb{F} = \mathbb{I} + \frac{\partial \mathbf{u}}{\partial \mathbf{X}}$, where $\mathbf{X}$ denotes the reference configuration of the sample).

The *magnetocrystalline anisotropy energy* is defined as

$$\mathcal{F}_{an} = \int_{\Omega_r} (1-\xi)\,\rho_r K_u \sin^2\theta dV \tag{2.37}$$

where K_u is called the *anisotropy constant*.

The *Zeeman energy* is

$$\mathcal{F}_{ze} = \int_{\Omega_r} -\mu_0 \rho_r \overline{\mathbf{M}} \cdot \mathbf{H}_a dV \tag{2.38}$$

where $\mathbf{H}_a$ is the external magnetic field and $\overline{\mathbf{M}}$ is the magnetization vector defined in (2.35).

The *magnetostatic energy* is

$$\mathcal{F}_{\text{sta}} = \int_{\Omega_r} -\mu_0 \rho_r \overline{\mathbf{M}} \cdot \mathbf{H}_d dV + \int_{\mathbb{R}^3} -\frac{\mu_0}{2} J \mathbf{H}_d \cdot \mathbf{H}_d dV \tag{2.39}$$

where $\mathbf{H}_d = -\mathbb{F}^{-T}\nabla(\Psi)$ is the *demagnetization field* induced by the magnetization of the MSMA sample and $J = \det(\mathbb{F})$. Here, Ψ is the scalar magnetic potential in $\mathbb{R}^3$ induced by the magnetization of the MSMA itself, as mentioned earlier. Ψ is assumed to be a continous function of X and regular at ∞.

The *mixture energy*, due to the micro interactions of the different martensitic variants and magnetic domains is

$$\begin{aligned} \mathcal{F}_{mix} &= \int_{\Omega_r} \rho_r f^{\xi}(\xi) dV \\ &+ \int_{\Omega_r} \rho_r \left[(1-\xi) f^{\alpha}\left(\frac{1}{2}\right) + \xi f^{\alpha}(\alpha) \right] dV \end{aligned} \tag{2.40}$$

where $f^{\xi}(\xi)$ and $f^{\alpha}(\alpha)$ are the energy densities that come from the mixture of the two variant states and the interactions of the different magnetic domains in each variant region.

The *potential energy of mechanical loading* is

$$\mathcal{F}_{ml} = \int_{\partial\Omega_r} -\mathbf{t}_A \cdot \mathbf{x} dA \tag{2.41}$$

where $\mathbf{t}_A$ is the external traction per unit area applied to the MSMA sample.

Finally, one needs to consider energy dissipation during the transformation of the material from variant 1 to variant 2. By assumption, for this model, the total energy dissipations during the transition can be written as

$$\mathcal{F}_{\text{dis}} = \pm \int_{\Omega_r} \int_{\xi_0(\mathbf{X})}^{\xi(\mathbf{X})} \rho_r \mathcal{D}^{\pm} d\tau dV \tag{2.42}$$

where $\xi_0(\mathbf{X})$ and $\xi(\mathbf{X})$ are the initial and final variant state distributions for the MSMA sample. $\mathcal{D}^{\pm}$ are positive functions called the dissipative resistances. For a MSMA transformation from variant 1 to variant 2, we have $\xi_0(\mathbf{X}) \leq \xi(\mathbf{X})$

and we take the " $+$ " dissipative resistance function. If the MSMA undergoes a transformation from variant 2 to variant 1, we have $\xi_0(\mathbf{X}) \geq \xi(\mathbf{X})$ and we take the " $-$ " dissipative resistance function.

Adding up (2.36) - (2.42) gives the total energy functional for the MSMA system. It is written explicitly as

$$\begin{aligned}\mathcal{G}(\mathbf{x},\Psi,\xi,\alpha,\theta;\mathbf{X}) &= \int_{\Omega_r} \rho_r \phi(\mathbb{F},\xi) dV \\ &+ \int_{\Omega_r} (1-\xi)\rho_r \left(K_u \sin^2\theta + f^\alpha\left(\frac{1}{2}\right)\right) dV \\ &+ \int_{\Omega_r} \rho_r f^\xi(\xi) dV + \int_{\Omega_r} \xi\rho_r f^\alpha(\alpha) dV \\ &+ \int_{\Omega_r} -\mu_0\rho_r \overline{\mathbf{M}}\cdot\mathbf{H}_a dV + \int_{\Omega_r} -\mu_0\rho_r\overline{\mathbf{M}}\cdot\mathbf{H}_d dV \\ &+ \int_{\mathbb{R}^3} -\frac{\mu_0}{2} J\mathbf{H}_d\cdot\mathbf{H}_d dV \pm \int_\Omega \int_{\xi_0(\mathbf{X})}^{\xi(\mathbf{X})} \rho_r \mathcal{D}^\pm d\tau dV \\ &- \int_{\partial\Omega_r} \mathbf{t}_A\cdot\mathbf{x} dA \end{aligned} \tag{2.43}$$

where the independent variables are $\mathbf{x}$ and Ψ, $\mathbf{x}$ being a point inside Ω_r.

2.3.2 Governing Equations for MSMAs Using Variational Methods

This subsection is dedicated to calculating the equations needed to determine the distribution of the scalar potential $\Psi(\mathbf{X})$ in $\mathbb{R}^3$. We will do this by making use of the calculus of variations and taking the variation of $\mathcal{G}$ in (2.42) with respect to Ψ. We will then set this equal to zero, requiring that $\mathcal{G}$ be stationary with respect to Ψ. This will naturally lead to two equations that can be used to solve for $\Psi(\mathbf{X})$ specific to the MSMA system. This work again comes from [12].

Firstly, the variation of the energy functional $\mathcal{G}$ with respect to the independant variable Ψ is

$$\begin{aligned}\delta_\Psi\mathcal{G} &= \delta_\Psi\left(\int_{\Omega_r} -\mu_0\rho_r\overline{\mathbf{M}}\cdot\mathbf{H}_d dV\right) \\ &+ \delta_\Psi\left(\int_{\mathbb{R}^3} -\frac{\mu_0}{2} J\mathbf{H}_d\cdot\mathbf{H}_d dV\right) \\ &= \int_{\Omega_r} \mu_0\rho_r(\mathbb{F}^{-1}\overline{\mathbf{M}})\cdot\nabla(\delta\Psi) dV \\ &- \int_{\mathbb{R}^3} \mu_0 J(\mathbb{C}^{-1}\nabla\Psi)\cdot\nabla(\delta\Psi) dV \end{aligned} \tag{2.44}$$

where $\mathbb{C}$ is defined in equation (2.21). This is because the terms in (2.43) that contain $\mathbf{H}_d$ are the only ones that depend on Ψ, through the definition of $\mathbf{H}_d$. One is free to define a ficticious displacement field in a region outside Ω_r, which is called Ω_r' such that $\mathbf{x}$ can be smoothly extended from Ω_r into its exterior [12]. Doing this enables the Lagrangian quantities to be defined outside of Ω_r.

Applying the divergence theorem to (2.44) in regions Ω_r and Ω_r' yields

$$\begin{aligned}\delta_\Psi\mathcal{G} = &-\int_{\Omega_r} \nabla\cdot(\mathbf{B}_l)\delta\Psi dV - \int_{\Omega_r'} \nabla\cdot(\mathbf{B}_l)\delta\Psi dV \\ &+ \int_{\partial\Omega_r} ([\mathbf{B}_l]\cdot\mathbf{N})\delta\Psi dS + \int_{\partial\Omega_\infty} (\mathbf{B}_l\cdot\mathbf{N})\delta\Psi dS, \end{aligned} \tag{2.45}$$

where

$$\mathbf{B}_l = \begin{cases} \mu_0(\rho_r\mathbb{F}^{-1}\overline{\mathbf{M}} - J\mathbb{C}^{-1}\nabla\Psi) & \text{in } \Omega_r \\ -\mu_0 J\mathbb{C}^{-1} & \text{in } \Omega_r', \end{cases} \tag{2.46}$$

and

$$[\mathbf{B}_l] = \mathbf{B}_l^i - \mathbf{B}_l^o \tag{2.47}$$

denotes the jump of the enclosed quantity in passing from the outside to the inside of the MSMA sample [12]. The last term in (2.45) vanishes because $\mathbf{B}_l \sim 1/|\mathbf{X}|^2$ as $|\mathbf{X}| \to \infty$ [12].

Since $\delta\Psi$ is arbitrary, in order for the energy functional $\mathcal{G}$ to be stationary with respect to Ψ, we must have

$$\nabla\cdot(\mathbf{B}_l) = 0 \tag{2.48}$$

in $\Omega_r \cup \Omega_r'$ and

$$[\mathbf{B}_l]\cdot\mathbf{N} = 0 \tag{2.49}$$

on $\partial\Omega_r$.

These two equations can be used to determine the distribution of the scalar potential $\Psi(\mathbf{X})$ in $\mathbb{R}^3$.

Aerospace Applications of SMAs

The use of Shape Memory Alloys in different fields of engineering is prevalent, and the aerospace sector is no exception [13]. SMAs are used in a wide variety of different aerospace applications for both aeronautical engineering and spaceflight, a few of which are discussed here. The central question in the aeronautical case is how to create aircraft that are more efficient in terms of flight capabilities and overall performance under any sort of flight conditions encountered. Somewhat in contrast and perhaps more exciting, the central question in the spaceflight case is how to create spacecraft that are capable of long distance space travel in order for humans to not only learn about the universe vicariously through rovers and telescopes, but to travel into deep space ourselves and leave the Earth for good. In both cases, SMA's play key roles in attempting to find solutions to these central questions as will be discussed in this section.

3.1 Wing Morphing

Commercial flights are one of the most widely used modes of transportation in today's world, especially when it comes to long distance travel. Airplanes rely on a combination of Newton's laws of motion and Bernoulli's principle in order to fly. Newton would say that there is a force of gravity pulling the airplane downward and therefore, if the plane wants to fly, there must be an opposing force that is greater than the force of gravity in the upward direction. This is called the *lift* force. An airplane generates a lift force thanks to its high speed and the shape of its wings. The *Camber* of a wing, loosely defined as the overall curvature or shape of the wing, is constructed in such a way to create a pressure difference between the air flowing on the top of the wing versus the air flowing underneath the wing, with the latter having a greater pressure than the former. Since there is more pressure from air flow underneath the wing than on top of the wing, there will be a lift force in the upward direction. Hence, the airplane can fly. However, airplanes face different flight conditions depending on a wide range of different factors such as where they are flying, what altitude they are at and how fast they are moving through the atmosphere. Wing morphing is the idea that the camber or shape of the wing is able to change by means of actuators, based on the different flight conditions the plane faces. This ensures that the flight is more aerodynamically efficient by maximizing the lift to drag ratio. In other words, by controlling the camber of a wing, airplanes are able to maximize their lift force and minimize their drag due to air resistance [14].

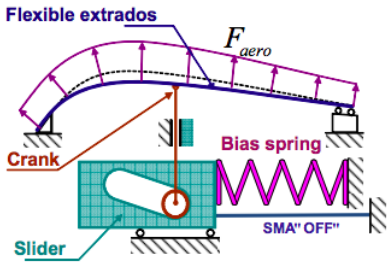

Figure 3.1: Schematic of wing morphing system on an aircraft wing. The shape of the flexible extrados changes depending on the position of the SMA slider [15].

In recent years, shape memory alloys were found to be one of the best materials for actuators used in aircraft to achieve camber control. The airfoil of a wing is defined as the cross-sectional shape of a wing. Changes in the camber of the airfoil are controlled by two SMA actuators located inside the wing itself. Figure 3.1 shows the mechanism that controls the camber of the airfoil and all its subsystems, including the SMA actuators. The SMA actuator is connected, via the bias spring, to the slider which in turn is connected to a crank. When the SMA is not active, the bias spring extends and pushes the slider and crank into their nominal position in the wing. Aerodynamic forces then force the flexible extrados, which are defined as the outer layers of the skin of the wing, upward [15]. When the aircraft is subjected to certain flight conditions, such as changes in temperature and atmospheric pressure, the SMA is activated and causes the bias spring to compress. This pulls the slider and crank to the right and changes the shape of the flexible extrados and hence morphs the wing into a different shape [15]. This mechanism for camber control, which is based on using SMAs for actuators, provides a way for airplanes to adapt to any variable aerodynamic forces and flight conditions and will in turn improve the efficiency of air travel in the future.

3.2 Mars Rover Tires

Recently, nitinol has been used in prototypes of a spring tire for future Mars rovers [16]. Current rovers make use of solid aluminium wheels which can be punctured by sharp rocks over time. The SMA spring tires were hence developed by NASA Glenn laboratories to make a long-lasting tire capable of withstanding the rough Martian surface. The spring tire exploits the pseudoelastic property of the SMA and the durability of the nitinol alloy. It is strong enough to support the 900 kg rover while deforming to roll smoothly over the terrain. Weight was also a key consideration due to the increased launch cost. The spring tires are relatively light compared to their solid counterparts, weighing in at just a few kilograms each. Hence, this advancement shows promise in helping to extend the lifetime and durability of future Mars rovers.

3.3 Solar Sail

In 1608, German astronomer Johannes Kepler observed a phenomenon that was quite unusual to him at the time. While observing a comet passing by the Sun, he noticed that the comet's tails were slightly displaced, as if they were blowing in the wind. He hypothesized that the comet's tails were indeed being blown by what he called "solar breeze". Influenced by this astonishing discovery, Kepler thought that one day we would be able to create ships with sails capable of riding this solar breeze, just as ordinary ships with sails ride the breeze of air on Earth. Of course, we know today that Kepler was correct and that the Sun does indeed give off solar wind in the form of charged particles. However in 1873, James Clerk Maxwell showed that sunlight itself could be used as a form of wind for a cosmic ship to use as propulsion. He demonstrated that particles of light, known as photons, exert a small amount of pressure when they collide with an object. This was later experimentally verified by Russian physicist Pyotr Lebedev in 1900 [17] and is the basis for how Solar Sails work.

The Solar Sail is a spacecraft that uses the momentum and pressure of solar photons as its mechanism for propulsion. Unlike regular propulsion methods that mix fuel and oxidizer together in a combustion reaction, the Solar Sail takes advantage of solar photons that collide with its sails after they are deployed, which accelerates the spacecraft towards its destination. Figure 3.2 is a depiction of what a Solar Sail spacecraft looks like. Because each photon only exerts a small amount of pressure on the sail, the sail itself must be quite large in order to have a high degree of propulsion. The method of deploying the sails has been a difficult challenge for engineers and scientists to overcome. There are limits to certain mechanisms of sail deployment such as high weight and overall complexity of deploying such large sails. In order to maximize the performance of the Solar Sail, it is crucial to have a deployment system that is lightweight and more efficient. Recently, experiments have shown that NiTi wires could be used as actuators for sail deployment, and would be effective in doing so [18].

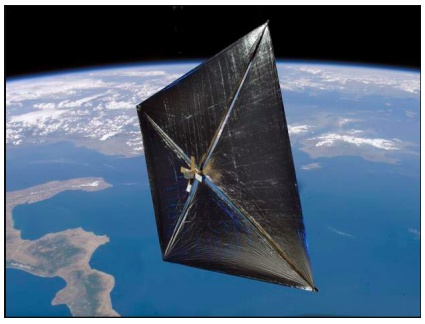

Figure 3.2: Depiction of the Solar Sail spacecraft. Retrieved from https://www.nasa.gov/mission_pages/tdm/solarsail/index.html

As shown in figure 3.3, small SMA wires made from NiTi are attached to the surface of the sail in certain configurations. The wires are then cooled down to their martensite phase, where they deform in such a way as to fold the sail up before deployment. Once the spacecraft is in space, heat from the Sun activates the SMA wires and they begin to deform back to their original austinsite phase. In doing so, the sails begin to deploy and open up and the spacecraft is ready to begin its journey through the Solar System.

The Solar Sail is an exciting part of the future of space exploration and travel, especially in its exploitation of an essentially inexhaustible fuel source. In the words of Carl Sagan: "*We have lingered long enough on the shores of the cosmic ocean. We are ready at last to set sail for the stars.*"

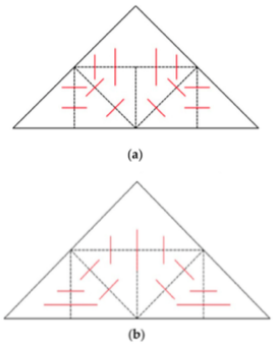

Figure 3.3: Two different SMA wire configurations for sail deployment. The red lines represent the wires. Retrieved from [18].

Numerical Model

4.1 Model Development

Auricchio and Pettrini [19] give a method for developing a three-dimensional model for stress-induced tranformation in SMAs in discrete and continuous time cases. We will briefly discuss the development of their continuous-time model, which is based on the methods described in Section 2.2.2. It is important to note that this model assumes only small strains in the material. This is acceptable because even in large deformations, oftentimes only small strains are induced. The model's constitutive relations are thermodynamically consistent, as they satisfy the second law of thermodynamics; in particular, the form common in continuum mechanics expressed by the Clausius-Duheim inequality,

$$D := D_{\text{me}} + D_{\text{th}} \geq 0. \tag{4.1}$$

Equation (4.1) dictates that the total mechanical and thermal dissipation D, (the specific internal entropy production) is necessarily greater than zero.[3]

The strain ε and absolute temperature T are used as control variables. The transformation tensor, $\mathbf{e}^{tr}$, describes the strain induced by phase transformations of the material. The free energy density function ψ for a polycrystalline SMA can be decomposed to get the following terms (as described in Equations (2.21) and (2.24)):

- The elastic strain energy from material deformation, defined as

$$\psi_{\text{el}} = \frac{K}{2}v^2 + G\left\|\mathbf{e} - \mathbf{e}^{tr}\right\|^2 - 3\alpha K v(T - T_0). \tag{4.2}$$

  As in Section 2.2.2, K is the bulk modulus, v is the volumetric strain (as in Equation 2.23), G the shear modulus, α the coefficient of thermal expansion, and T_0 an initial temperature.

- The chemical energy from martensitic transformation, given by

$$\psi_{\text{ch}} = \beta\langle T - M_{\text{f}}\rangle\left\|\mathbf{e}^{tr}\right\|, \tag{4.3}$$

  where β is a coefficient relating the critical stress and temperature. The angled brackets denote that we only consider the positive part of $T - M_{\text{f}}$ (as described in [19]). In analogy to Equation (2.24), we note here that $f(T) := \beta\langle T - M_{\text{f}}\rangle$ which depends only on the temperature.

- The transformation strain energy,

$$\psi_{\text{tr}} = \frac{H}{2}\left\|\mathbf{e}^{tr}\right\|^2, \tag{4.4}$$

  where H is the hardening parameter mentioned in Section 2.2.2.

- The free energy absorbed or released by a change in temperature (relative to T_0),

$$\psi_{\text{id}} = (u_0 - T\eta_0) + c\left[(T - T_0) - T\ln\frac{T}{T_0}\right], \tag{4.5}$$

  assuming an ideal incompressible solid, where c is the specific heat capacity, u_0 the internal energy at T_0, and η_0 the entropy at T_0.

- The indicator function $\mathscr{I}(\mathbf{e}^{tr})$ defined as in Equation (2.22) above.

Summing all of the above together, we obtain our original convex free energy function,

$$\psi(v, \varepsilon, \mathbf{e}^{tr}, T) = \psi_{\text{el}} + \psi_{\text{ch}} + \psi_{\text{tr}} + \psi_{\text{id}} + \mathscr{I}(\mathbf{e}^{tr}). \tag{4.6}$$

We can therefore obtain our four constitutive equations. For the continuous-time model, these are given by

$$\begin{aligned}
p &= \frac{\partial\psi}{\partial v} = K\left[v - 3\alpha(T - T_0)\right], \\
\mathbf{S}_{\text{dev}} &= \frac{\partial\psi}{\partial\mathbf{e}} = 2G(\mathbf{e} - \mathbf{e}^{tr}), \\
\eta &= -\frac{\partial\psi}{\partial T} = \eta_0 + 3\alpha K v - \beta\left\|\mathbf{e}^{tr}\right\|\frac{\langle T - M_{\text{f}}\rangle}{|T - M_{\text{f}}|} + c\ln\frac{T}{T_0}, \\
\mathbf{X} &= -\frac{\partial\psi}{\partial\mathbf{e}^{tr}} = \\
&\quad \mathbf{S}_{\text{dev}} - \left[\beta\langle T - M_{\text{f}}\rangle + H\left\|\mathbf{e}^{tr}\right\| + \partial\mathscr{I}(\mathbf{e}^{tr})\right]\partial\mathbf{e}^{tr}.
\end{aligned} \tag{4.7}$$

Here, we have that p is the volumetric part of the stress $\boldsymbol{\sigma}$ (i.e., pressure), $\mathbf{S}_{\text{dev}}$ is the deviatoric part thereof, η is the entropy, and the second-order tensor $\mathbf{X}$ is the thermodynamic force due to strain; a kind of relative stress. The derivatives

$\partial\mathscr{I}(\mathbf{e}^{tr})$ and $\partial\mathbf{e}^{tr}$ in the definition of $\mathbf{X}$ Equation (4.7) are defined in Equation (2.32). We define the evolution of $\mathbf{e}^{tr}$ as

$$\dot{\mathbf{e}}^{\mathrm{tr}} = \dot{\zeta}\frac{\partial F(\mathbf{X})}{\partial \boldsymbol{\sigma}}, \tag{4.8}$$

with the Kuhn-Tucker optimality conditions

$$\dot{\zeta} \geq 0, \qquad F \geq 0, \qquad \text{and} \quad \dot{\zeta}F = 0. \tag{4.9}$$

The limit function, F, is given by

$$F(\mathbf{X}) = \sqrt{2J_2} + m\frac{J_3}{J_2} - R, \tag{4.10}$$

where m is a material parameter, J_2, J_3 are invariants of $\mathbf{X}$ of the second and third order respectively, and R is the radius of elastic domain.

Equations (4.7), (4.8), (4.9), and (4.10), constitute the time-continuous model for the SMA.

4.2 Computational SMA Model

Smith and Massad developed a Homogenized Energy Model for SMAs in Matlab [20].

```
m=matparam(1);
c=comparam(m);
[sig,ep,T,xm,xp,tspan] = polycryst(0:400,
  input_Te(0),m,c);
```

Listing 4.1: Contents of main file

4.2.1 Setup

The model is first initialized using the provided material parameters in `matparams.m`. It takes in 19 unique material parameters, some of which include the volume density, specific heat capacity, as well as resistivities, temperatures, thermal expansions, and key temperatures for the martenite and austenite phases. Out of the box, the code is set up to simulate Nitinol.

Next, additional key parameters are computed and assigned in the `comparams.m` script. From these, the model can be developed.

The script `polycryst.m` sets up the polycrystal homogenization model. This comprises two functions: the first is called `polycryst`, and the second is `integrand`.

```
function [sig,ep,T,xm,xp,tspan] = polycryst(
    tspan,Tini,mparams,cparams)
```

Listing 4.2: Polycryst function parameters

The first input parameter (`tspan`) is chosen to be the range from 0 to 400 discrete seconds. This is long enough to obtain a full hysteresis loop in the generated plots. The input temperature is calculated through another script titled `input_Te`, which returns an input temperature based on the current time value. The last two input parameters are simply derived from `matparams` and `comparams`.

4.2.2 Algorithm

Next, the function sets up a double integral computation using a 4-point Gauss-Legendre Quadrature method. Smith describes the method in [3] as a method for numerically evaluating integrals over $D = [-1,1] \times [-1,1]$ using Legendre polynomials,

$$P_n(x) = \frac{1}{2^n n!}\frac{\mathrm{d}^n}{\mathrm{d}x^n}\left(x^2-1\right)^n, \; n = 0,1,2,\ldots \tag{4.11}$$

To approximate the integral of a 2-D function $f(x,y)$, we can take the sum

$$\int_a^b\int_c^d f(x,y)\,\mathrm{d}x\mathrm{d}y \approx \sum_{i=1}^{n_x}\sum_{j=1}^{n_y} f(x_i,y_i)w_i w_j, \tag{4.12}$$

where x_i, y_i are the roots of the n^{th} Legendre polynomial P_n described above (in this case, we are interested in P_4), and w_i, w_j are simply weights which can be obtained from a reference table. In the model SMA code, these constants can be obtained by calling a function in `gweights.m`. Note that we can do a transformation to set the domain of integration to $[-1,1] \times [-1,1]$ to satisfy the requirements.

```
%%Double Integration
tic;
Fy = zeros(4,length(tspan));
FyT=Fy; Fym = Fy;  Fyp = Fy;
funx = Fy; funy=Fy;    funxT = Fy; funyT=Fy;
funxm = Fy; funym=Fy;  funxp = Fy; funyp=Fy;
ep=zeros(size(tspan)); T=ep; xm=ep; xp=ep;
for jy = 1:numsub
    ysub = gnodes(jy,numsub,y0,y1);
    for inodey = 1:4  %y Subintervals
        sigef = ysub(inodey);

        %x Integration
        Fx = repmat(0,size(funx));     FxT =
    repmat(0,size(funxT));
        Fxm = Fx;      Fxp = Fx;
        for jx = 1:numsub
            xsub = gnodes(jx,numsub,x0,x1);
            for inodex = 1:4 %x Subintervals
                dsig = xsub(inodex);
    [ep,T,xm,xp] = integrand(dsig,sigef,tspan,
    Tini,mparams,cparams,lgmu,lgvar,sevar);
    funx(inodex,:) = ep;  funxT(inodex,:) = T;
    funxm(inodex,:) = xm; funxp(inodex,:) = xp;
   end
            Fx = Fx + funx; %4xlength(tspan)
    Matrix
```

```
            FxT = FxT + funxT; %4xlength(tspan) Matrix
   Fxm = Fxm + funxm;  Fxp = Fxp + funxp;
        end %End x integration

        funy(inodey,:) = gw'*Fx; %1xlength(tspan) Vector
        funyT(inodey,:) = gw'*FxT; %1xlength(tspan) Vector
        funym(inodey,:) = gw'*Fxm;  funyp(inodey,:) = gw'*Fxp;
    end
    Fy = Fy + funy; %4xlength(tspan) Matrix
    FyT = FyT + funyT; %4xlength(tspan) Matrix
Fym = Fym + funym;  Fyp = Fyp + funyp;
end
```

Listing 4.3: Snippet of main integrationn loop

The code then iterates over each set node to evaluate the energy function integrand, each time recomputing the required parameters, as shown in 4.3.

```
function [ep,T,xm,xp] = integrand(dsig,sigef,tspan,Tini,mparams,cparams,lgmu,lgvar,sevar)
```

Listing 4.4: Integrand function parameters

The `integrand` function is called in this loop to update the integrand. Put simply, the function outputs the strain output vector `ep`, internal temperature vector `T`, and the M^+, M^- phase vectors `xp`, `xm`. With this, we can recompute our parameters and solve for the energy function.

4.2.3 Results

Finally, the code generates plots of the results using the `Plotfun.m` script. Four different plots are outputted, seen in Figures 4.1 and 4.2.

The top plot in figure 4.1 shows the fraction of the solid in each state (austentite in red and martensite in blue). The lower plot in figure 4.1 shows how the temperature of the solid changes as the system evolves in time. The minimum temperature is attained at $t \approx 180\,\text{s}$, when the material is entirely in the martensite state. As the temperature rises agin to a peak, the solid returns to its austenite configuration. Phase transitions occur at the critical stresses σ_M and σ_A, whose values depend on the parameters used.

The top plot in figure 4.2 shows a clear hysteresis loop in the stress-strain curve. The material begins at minimum stress and strain in the bottom left. Initially, as the stress increases, so does the strain with it. Once the critical strain is reached, we see the hysteretic behaviours begin to appear.

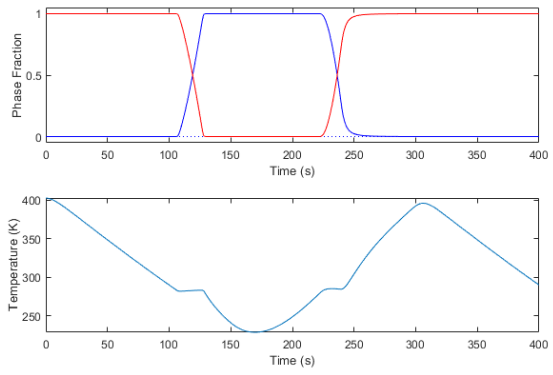

Figure 4.1: Temperature evolution of the system in time (top). Proportion of the solid in austentite and martensite phases (bottom).

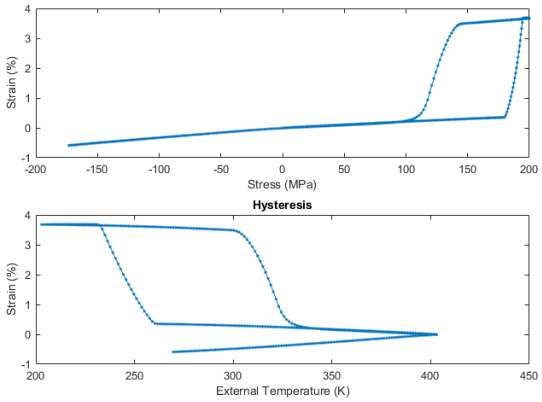

Figure 4.2: Stress-strain and temperature-strain curves generated by the SMA model for Nitinol. Both curves clearly show hysteretic behaviour.

Conclusion

Shape Memory Alloys are a very fascinating subclass of smart materials. The hallmark of these materials is the shape memory effect, which enables them to make transitions from one solid phase of matter to another while "remembering" the original state they were in. Transitions of SMAs between the *martensite* and *austensite* phases can be induced through temperature changes, external applied stresses and even being subjected to the presence of a magnetic field, in the case of magnetic SMAs.

Techniques from the calculus of variations are useful when modeling SMAs from a mathematical standpoint. Whether in a Homogenized Energy, Entropy-Gradient, or magnetic SMA model, the free energy can be formulated as a functional, the variations of which yield the constitutive equations that dictate the material behaviour. Using calculus of variations, it is possible to use these materials as primitive computers, giving them roles in impressive moments of science, such as their application in the Mars Rover. Due to their shape memory quality, special consideration is given to the thermomechanical coupling of these materials to accurately simulate their dynamics.

We have also breifly discussed a few of the many applications for SMAs used in the aerospace industry. These included *Wing Morphing* where a shape memory alloy was used to craft airplane wings in such a way as to allow them adapt to various flight conditions on their own, making for an increase in the quality of air travel, *Mars Rover Tires* where SMA's were used to craft prototypes of high quality tires that can endure rough terrain on the surface of Mars by making use of the pseudoelastic effect, and *Solar Sails* where SMAs were used as a deployment mechanism for the sails on this spacecraft, so that it can be propelled entirely by solar photons.

Acknowledgements

We are grateful to Ralph Smith for his comprehensive book on modeling smart materials. We also thank Dr. Francis Poulin for providing us with some sample codes which helped us get started. Finally, we want to thank Dr. Morris for her guidance, support and encouragement in conducting this project.

List of Figures

Bibliography

[1] G. Kauffman and I. Mayo, "Memory metal," *Chem Matters*, vol. 11, p. 4, 1993.

[2] I. Mayo, "Metal with memory," 1993.

[3] R. C. Smith, *smart material systems: model development*. SIAM, 2005.

[4] K. Morris, "What is hysteresis?," *Applied Mechanics Reviews*, vol. 64, no. 5, 2011.

[5] K. Morris, *AMATH 456 Course Notes*. University of Waterloo, 2020.

[6] S. Blundell and K. Blundell, *Concepts in Thermal Physics*. OUP Oxford, 2010.

[7] H. Callen, *Thermodynamics and an Introduction to Thermostatistics*. Wiley, 1985.

[8] F. Auricchio, E. Boatti, A. Reali, and U. Stefanelli, "Gradient structures for the thermomechanics of shape-memory materials," *Computer Methods in Applied Mechanics and Engineering*, vol. 299, pp. 440–469, 2016.

[9] P. Webster, K. Ziebeck, S. Town, and M. Peak, "Magnetic order and phase transformation in Ni2MnGa," *Philosophical Magazine B*, vol. 49, no. 3, pp. 295–310, 1984.

[10] K. Ullakko, J. Huang, C. Kantner, R. O'handley, and V. Kokorin, "Large magnetic-field-induced strains in Ni2MnGa single crystals," *Applied Physics Letters*, vol. 69, no. 13, pp. 1966–1968, 1996.

[11] R. Tickle and R. D. James, "Magnetic and magnetomechanical properties of Ni2MnGa," *Journal of Magnetism and Magnetic Materials*, vol. 195, no. 3, pp. 627–638, 1999.

[12] J. Wang and P. Steinmann, "A variational approach towards the modeling of magnetic field-induced strains in magnetic shape memory alloys," *Journal of the Mechanics and Physics of Solids*, vol. 60, no. 6, pp. 1179–1200, 2012.

[13] G. Costanza and M. E. Tata, "Shape memory alloys for aerospace, recent developments, and new applications: A short review," *Materials*, vol. 13, no. 8, p. 1856, 2020.

[14] S. Barbarino, O. Bilgen, R. M. Ajaj, M. I. Friswell, and D. J. Inman, "A review of morphing aircraft," *Journal of intelligent material systems and structures*, vol. 22, no. 9, pp. 823–877, 2011.

[15] V. Brailovski, P. Terriault, T. Georges, and D. Coutu, "SMA actuators for morphing wings," *Physics Procedia*, vol. 10, pp. 197–203, 2010.

[16] "Reinventing the wheel," *NASA*, Oct 2017. Available at https://www.nasa.gov/specials/wheels/.

[17] P. Lebedev, "Investigations on the pressure forces of light," *Annals of Physics*, vol. 6, pp. 433–458, 1901.

[18] G. Bovesecchi, S. Corasaniti, G. Costanza, and M. E. Tata, "A novel self-deployable solar sail system activated by shape memory alloys," *Aerospace*, vol. 6, no. 7, p. 78, 2019.

[19] F. Auricchio and L. Petrini, "A three-dimensional model describing stress-temperature induced solid phase transformations: solution algorithm and boundary value problems," *International journal for numerical methods in engineering*, vol. 61, no. 6, pp. 807–836, 2004.

[20] R. C. Smith and J. E. Massad, "Homogenized energy model for SMA." https://rsmith.math.ncsu.edu/smart_Material_Systems/Chapter5/, 2004.